Heteronuclear d-d and d-f Ru(II)/M complexes [M = Gd(III), Yb(III), Nd(III), Zn(II) or Mn(II)] of ligands combining phenanthroline and aminocarboxylate binding sites: combined relaxivity, cell imaging and photophysical studies.

Bethany J. Crowston, James D. Shipp, Dimitri Chekulaev, Luke K. McKenzie, Callum Jones, Julia A. Weinstein, Anthony J. H. Meijer, Helen E. Bryant, Louise Natrajan, Adam Woodward and Michael D. Ward*

Experimental Supporting Information

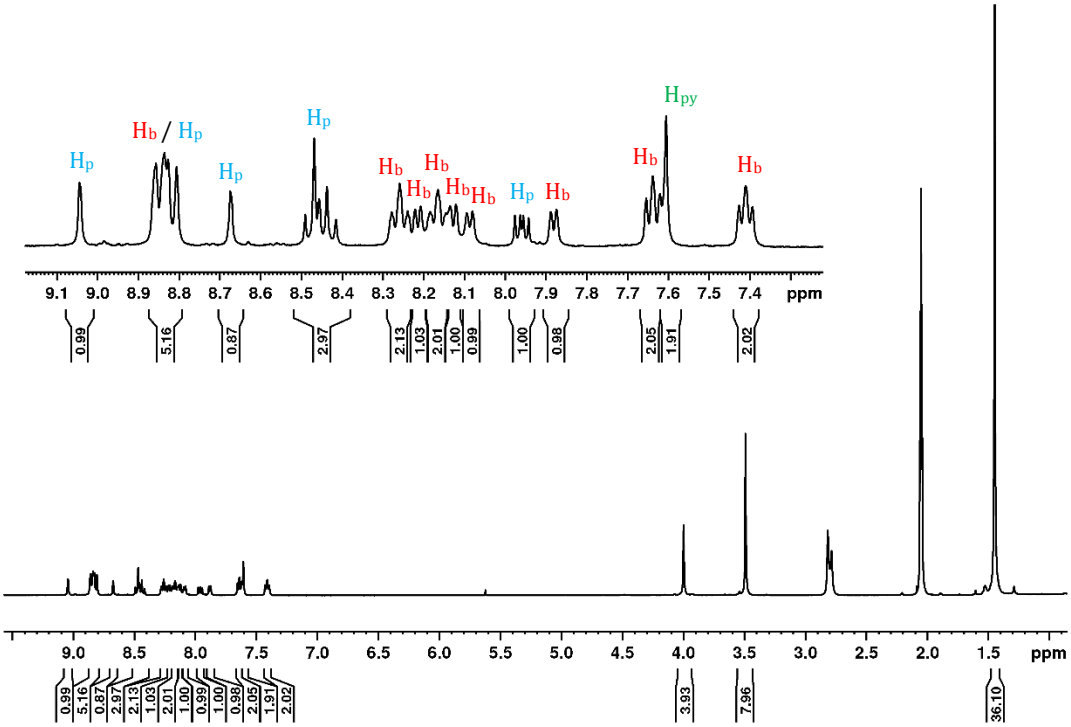

Fig. S1. ^{1}H NMR spectrum (400 MHz, d6-acetone) of **Ru•E**. H_b = Proton on bipyridine ligand; H_p = proton on phenanthroline ligand; H_{py} = proton on pyridine ring.

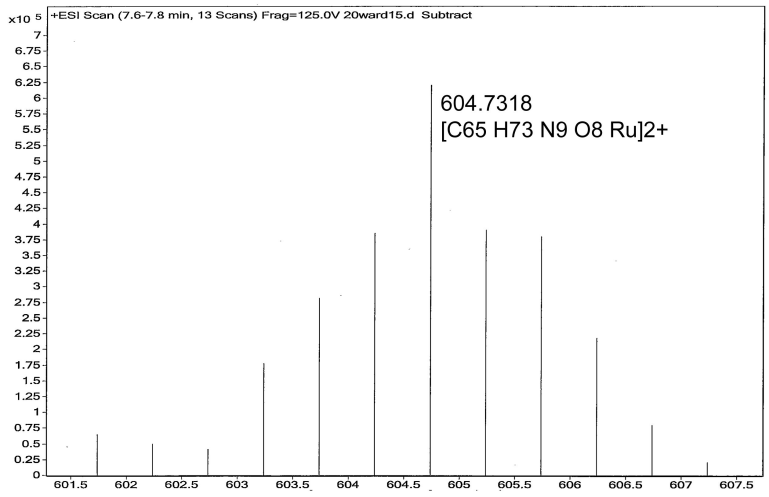

Fig. S2. High-resolution ES mass spectrum of **Ru•E**

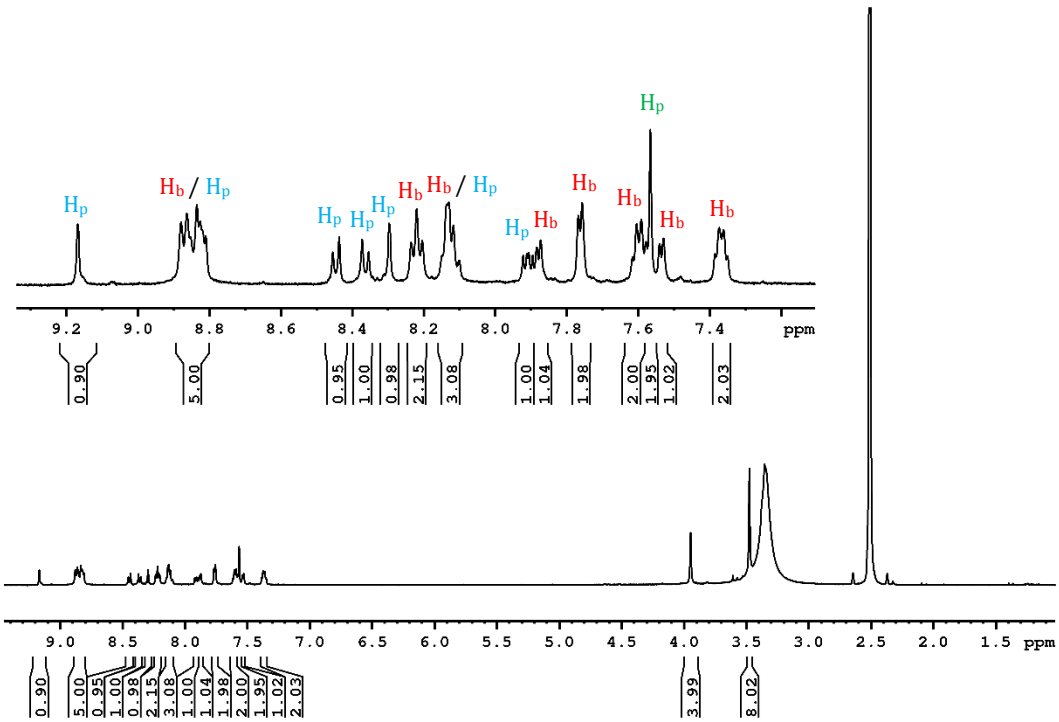

Fig. S3. ^{1}H NMR spectrum (500 MHz, d6-DMSO) of **Ru•L**. H_b = Proton on bipyridine ligand; H_p = proton on phenanthroline ligand; H_{py} = proton on pyridine ring.

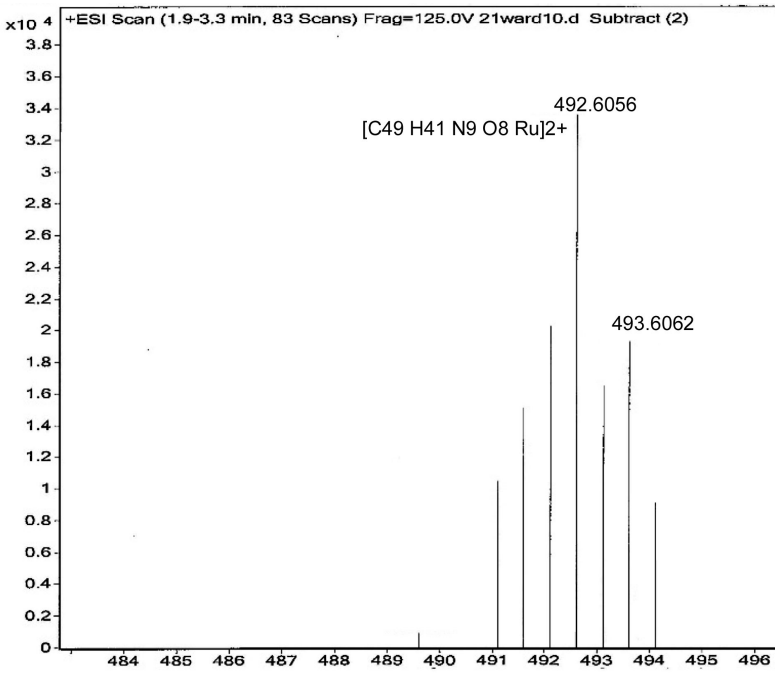

Fig. S4. High-resolution ES mass spectrum of **Ru•L**

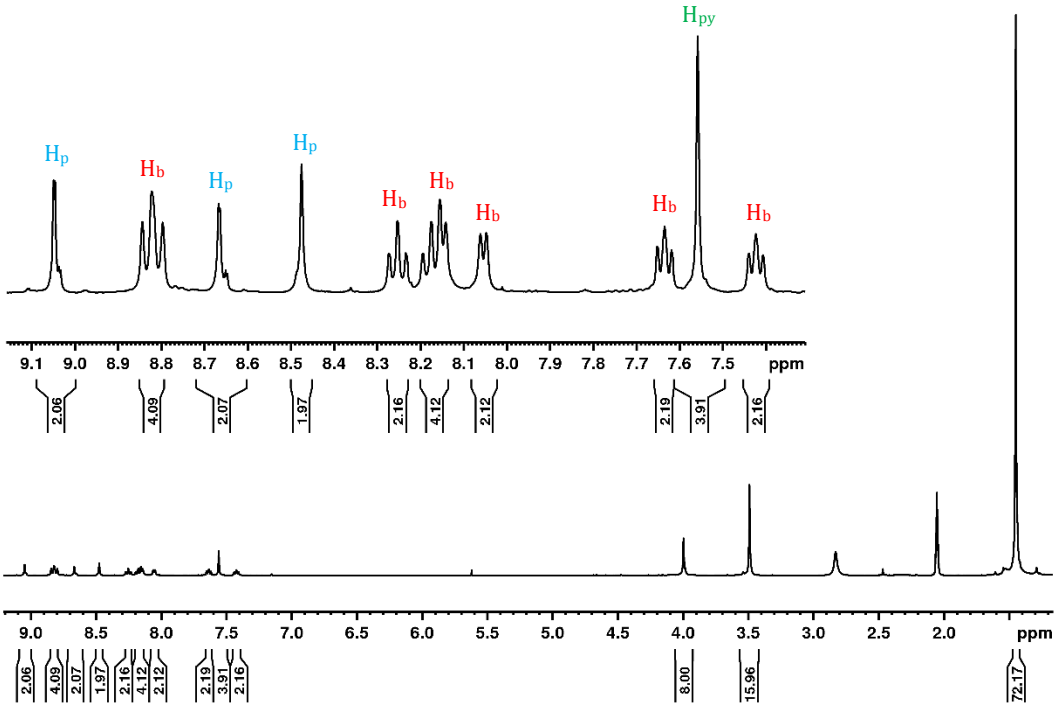

Fig. S5. ^{1}H NMR spectrum (400 MHz, d_6-acetone) of **Ru•E$_2$** at 298 K. H_b = proton on bipyridine ligand, H_p = proton on phenanthroline ligand, H_{py} = proton on pyridine ring.

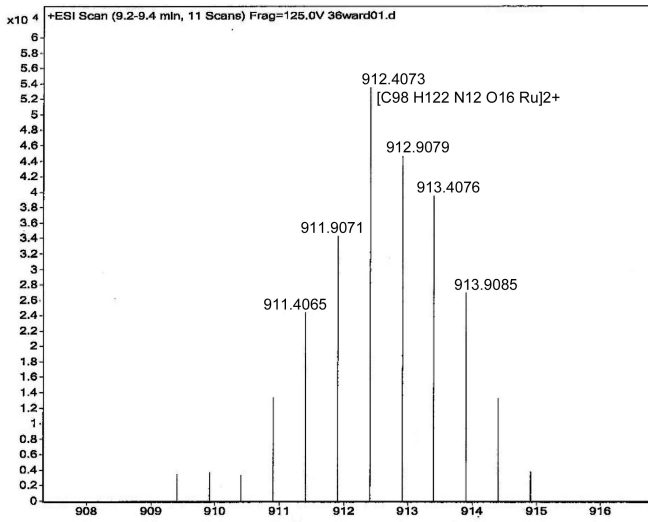

Fig. S6 High-resolution ES mass spectrum of **Ru•E$_2$**

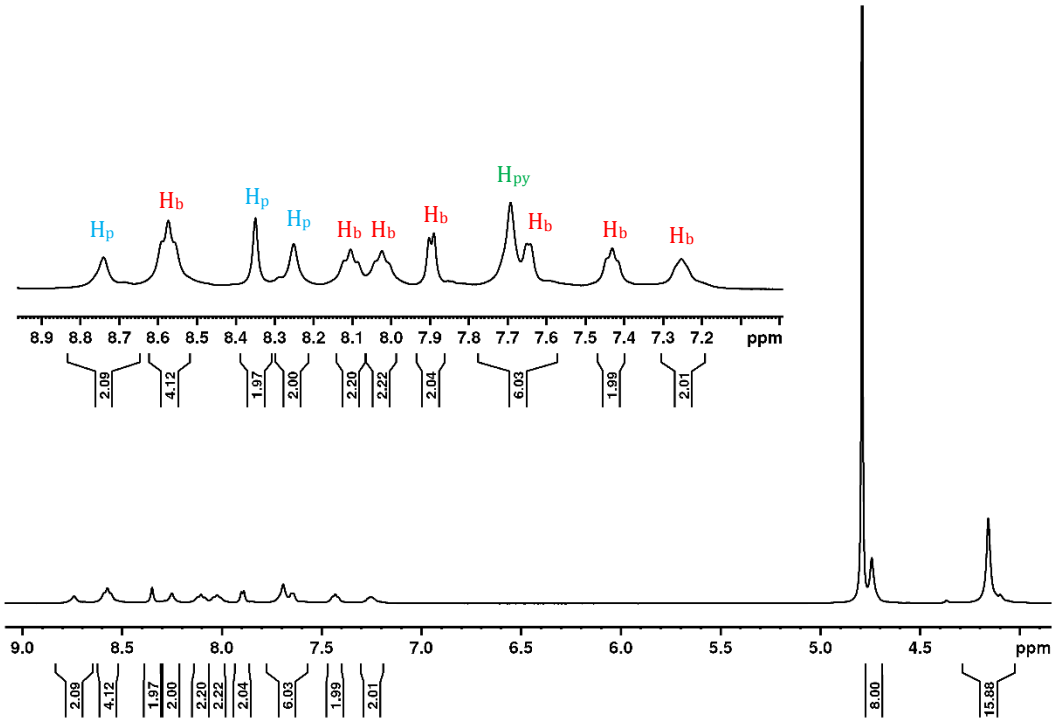

Fig. S7. ^{1}H NMR spectrum (400 MHz, D_2O) of **Ru•L$_2$** at 298 K. H_b = proton on bipyridine ligand, H_p = proton on phenanthroline ligand, H_{py} = proton on pyridine ring.

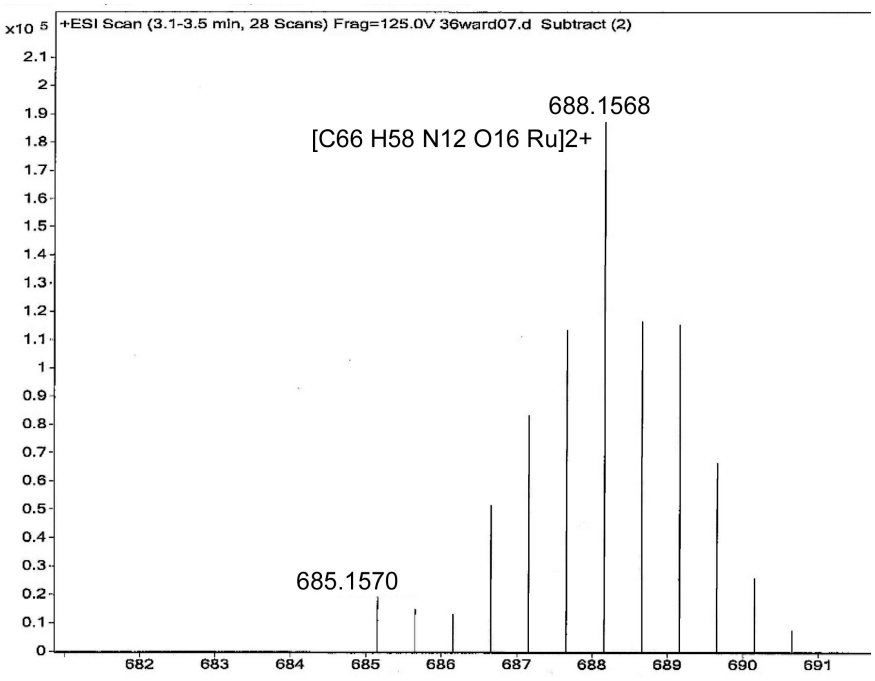

Fig. S8. High-resolution ES mass spectrum of **Ru•L$_2$**

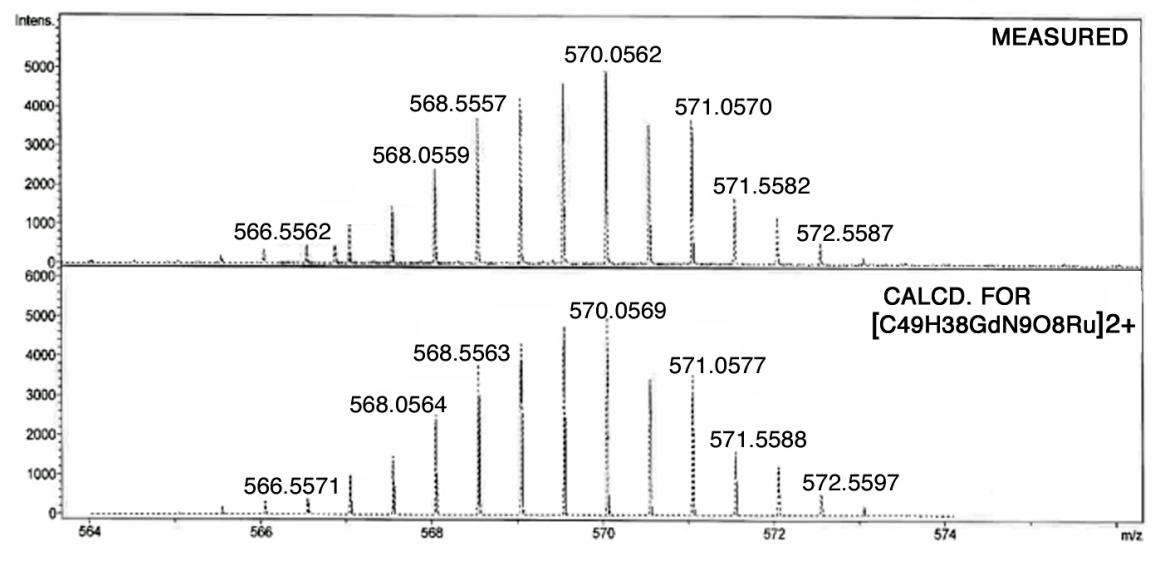

Fig. S9. Part of the high-resolution ES mass spectrum of **Ru•Gd** showing (top) observed and (below) calculated signals for $[C_{49}H_{37}N_9O_8RuGd + H]^{2+}$

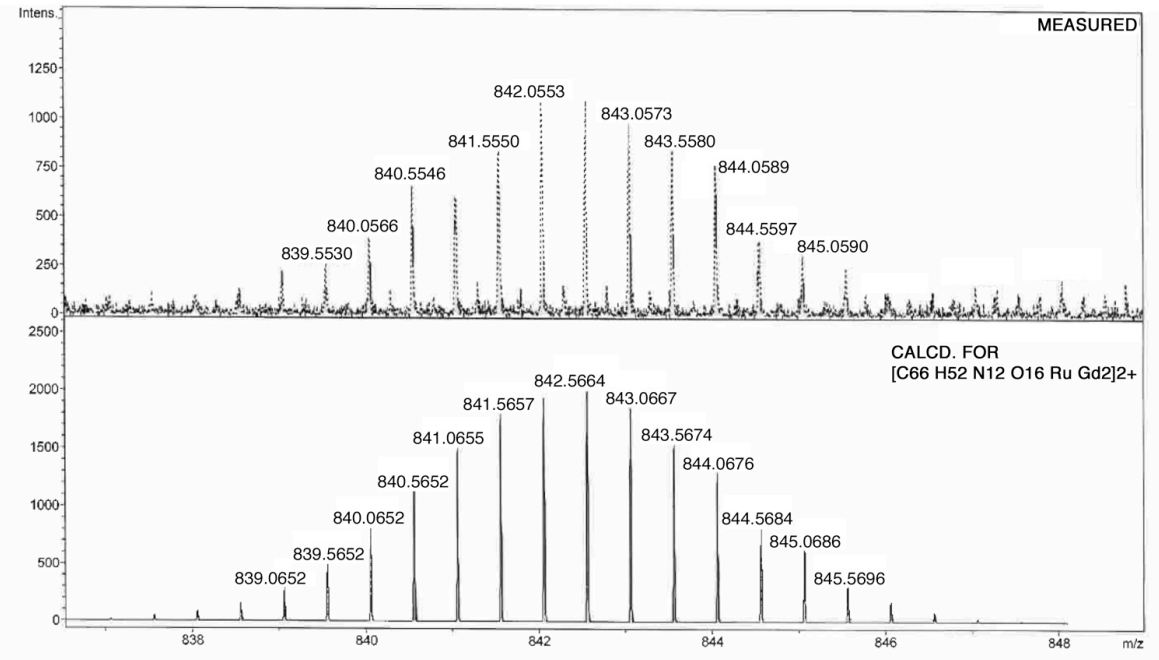

Fig. S10. Part of the high-resolution ES mass spectrum of **Ru•Gd$_2$** showing (top) observed and (bottom) calculated signals for $[C_{66}H_{50}N_{12}O_{16}RuGd_2+2H]^{2+}$

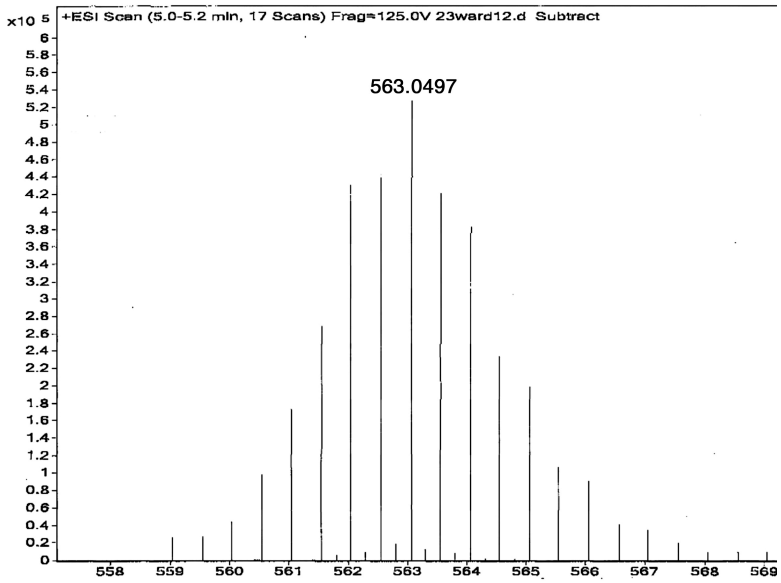

Fig. S11. Part of the high resolution ES mass spectrum of **Ru•Nd** showing the signal for $[C_{49}H_{37}N_9O_8RuNd + H]^{2+}$.

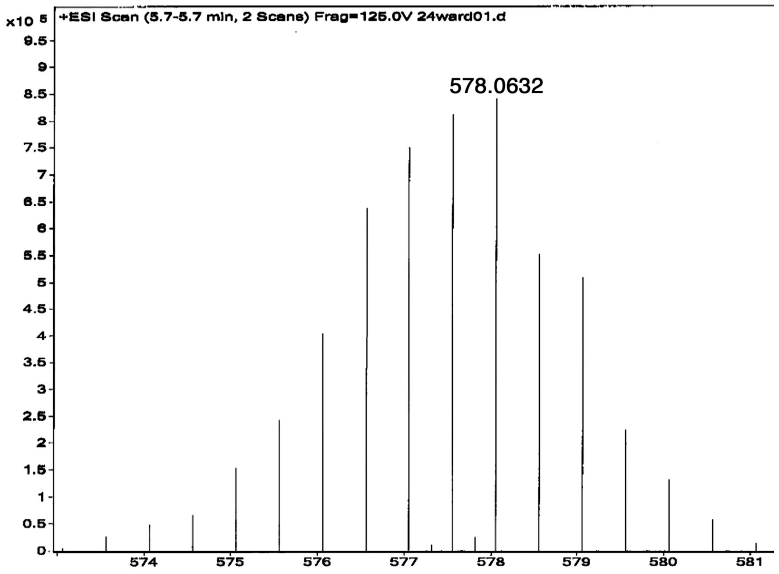

Fig. S12. Part of the high resolution ES mass spectrum of **Ru•Yb** showing the signal for $[C_{49}H_{37}N_9O_8RuYb + H]^{2+}$.

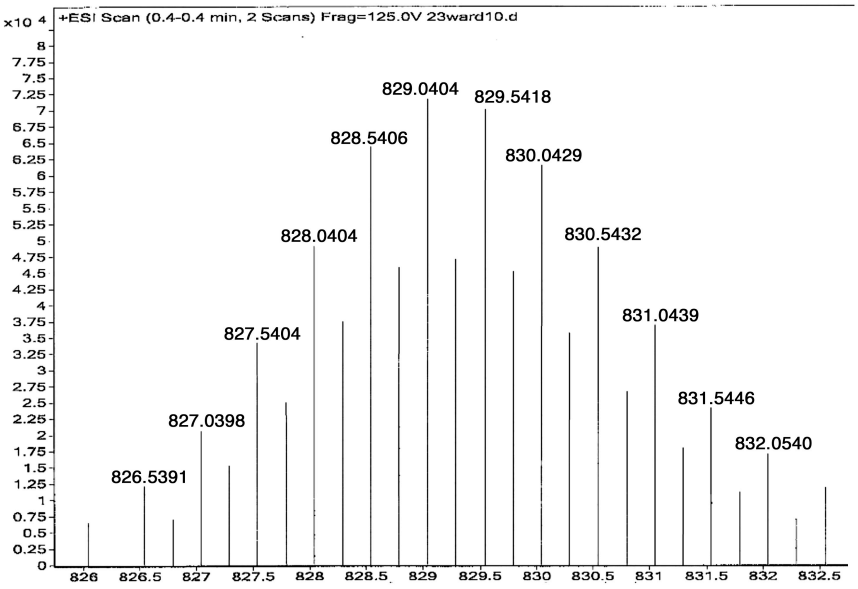

Fig. S13. Part of the high resolution ES mass spectrum of **Ru•Nd$_2$** showing the signal for $[C_{66}H_{50}N_{12}O_{16}RuNd_2 + 2H]^{2+}$.

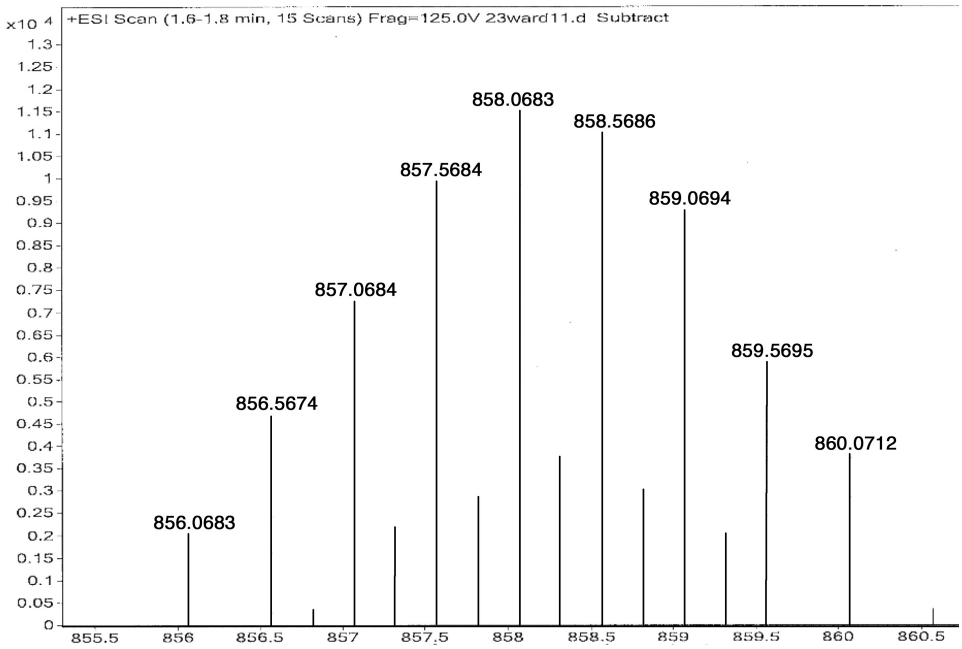

Fig. S14. Part of the high resolution ES mass spectrum of **Ru•Yb$_2$** showing the signal for $[C_{66}H_{50}N_{12}O_{16}RuYb_2 + 2H]^{2+}$.

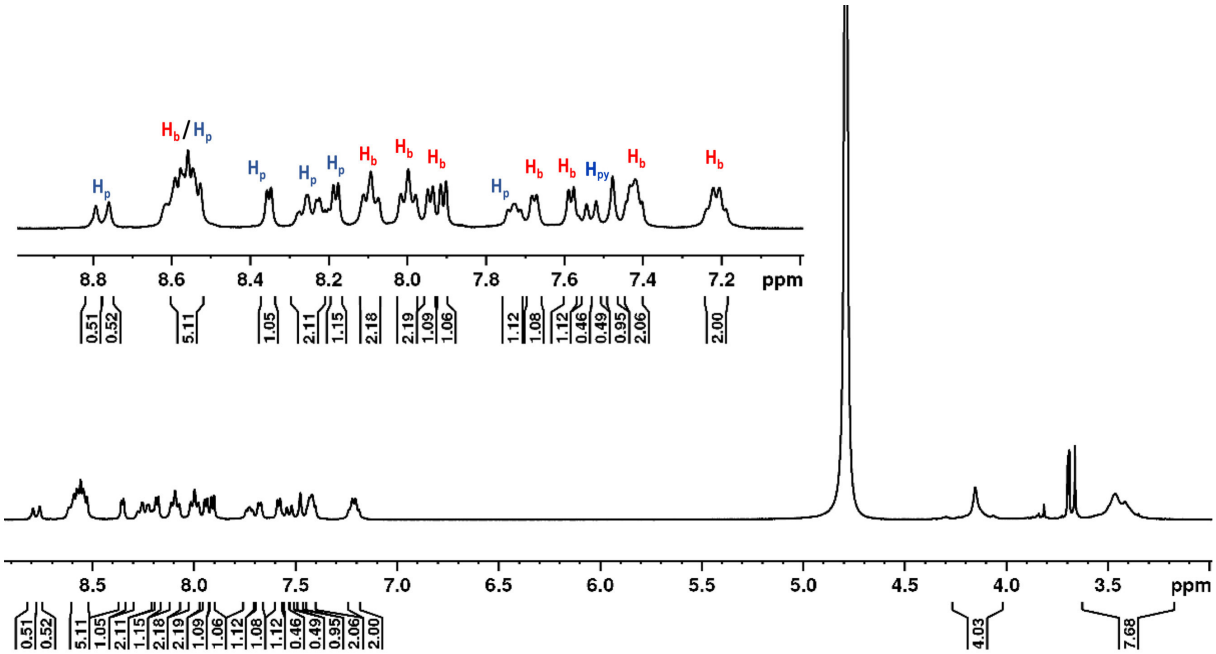

Fig. S15. ^{1}H NMR spectrum (400 MHz, D_2O) of **Ru•Zn** at 298 K. (H_b = proton on bipyridine ligand, H_p = proton on phenanthroline ligand, H_{py} = proton on pyridine ring).

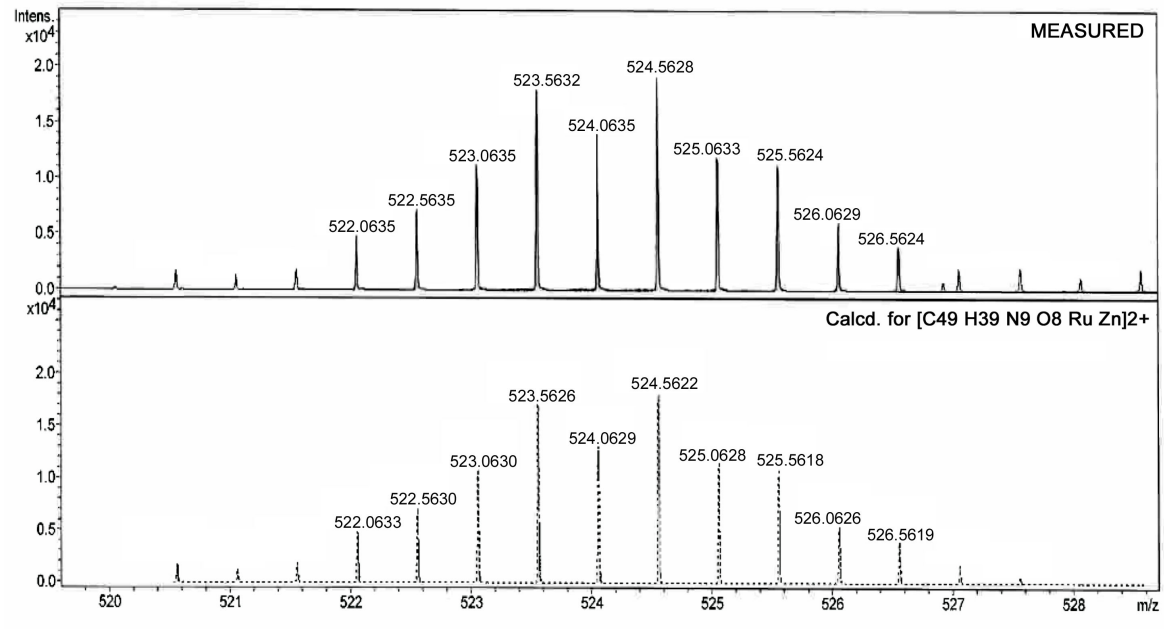

Fig. S16. Part of the high resolution ES mass spectrum of **Ru•Zn** showing the signal for $[C_{49}H_{37}N_9O_8RuZn+2H]^{2+}$.

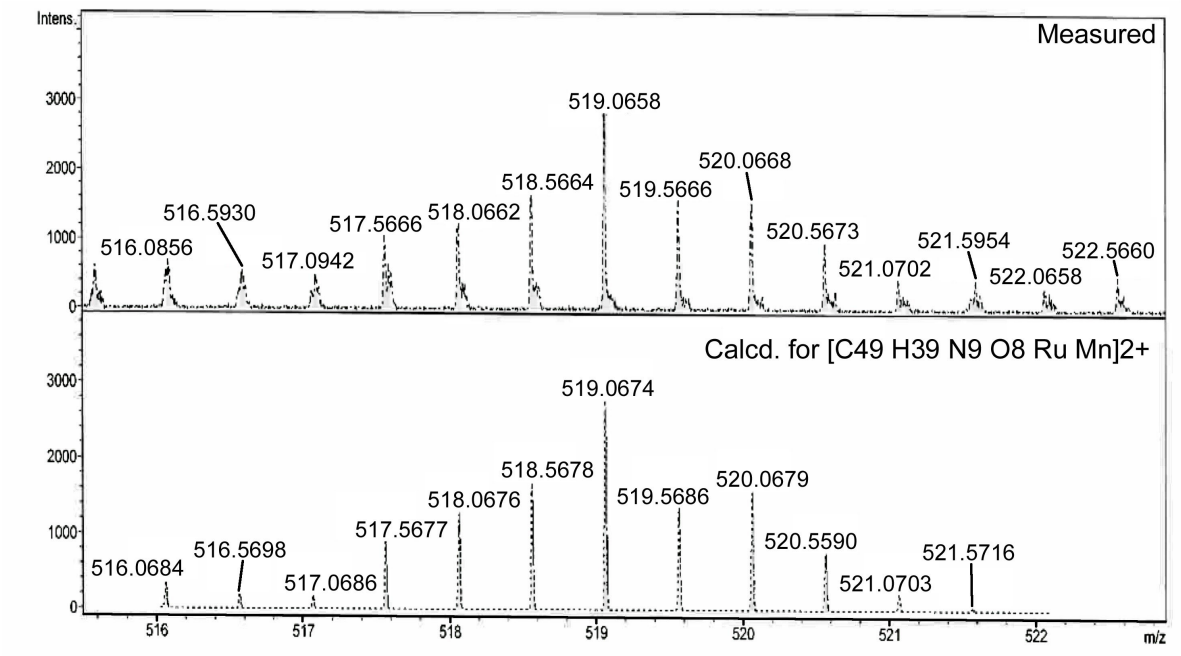

Fig. S17. Part of the high resolution ES mass spectrum of **Ru•Mn** showing the signal for $[C_{49}H_{37}N_9O_8RuMn+2H]^{2+}$.

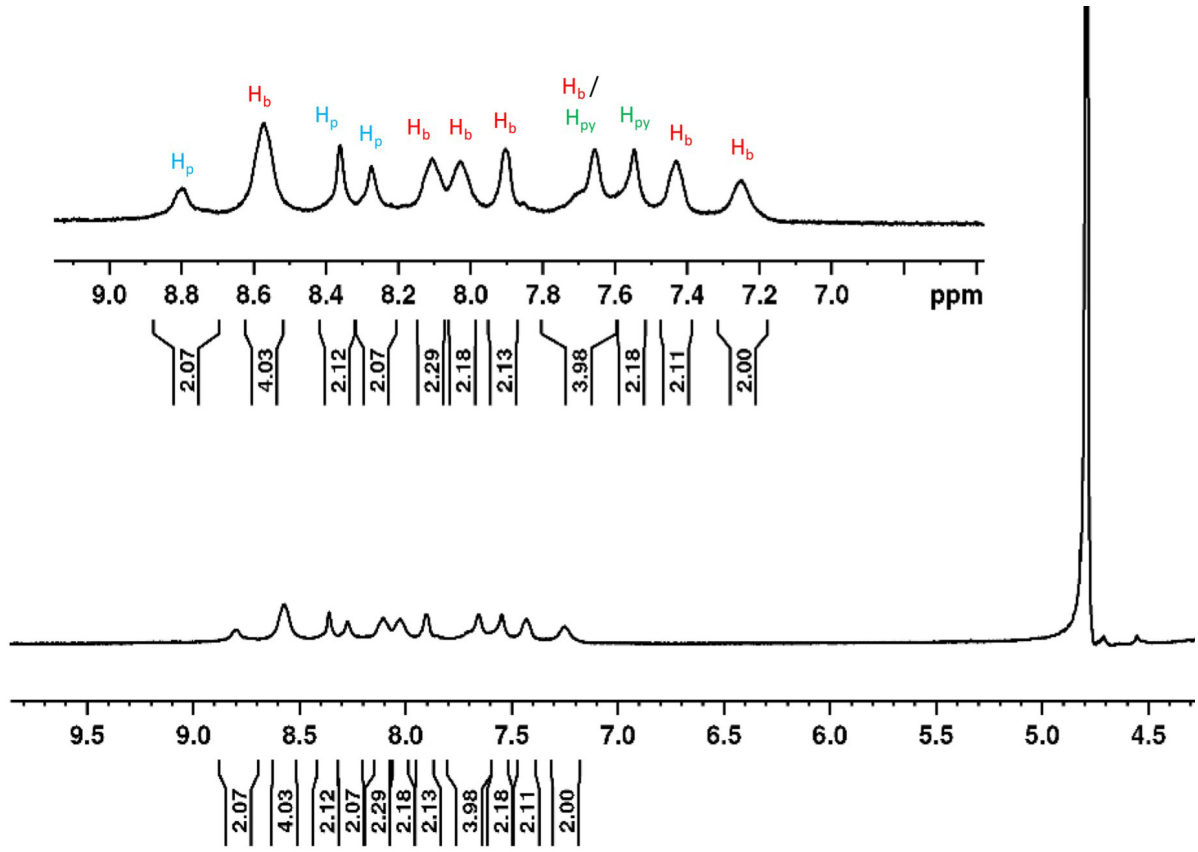

Fig. S18. ^{1}H NMR spectrum (400 MHz, D_2O) of **Ru•Zn$_2$** at 298 K. (H_b = proton on bipyridine ligand, H_p = proton on phenanthroline ligand, H_{py} = proton on pyridine ring).

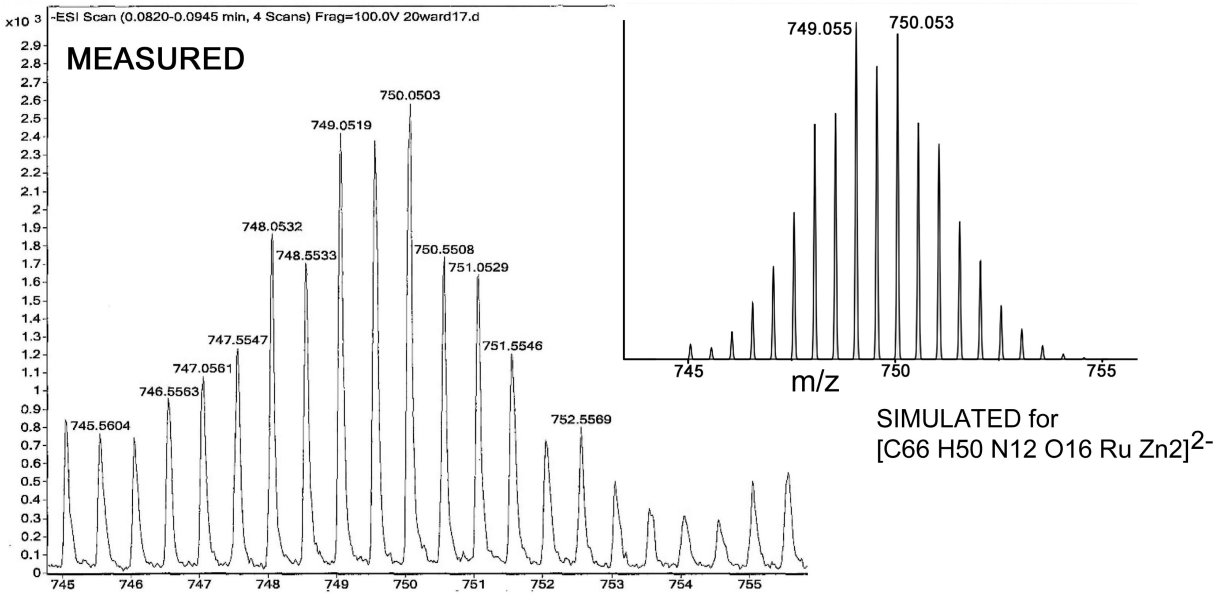

Fig. S19. Part of the high resolution ES mass spectrum of **Ru•Zn$_2$** showing the signal for $[C_{66}H_{50}N_{12}O_{16}RuZn_2]^{2-}$.

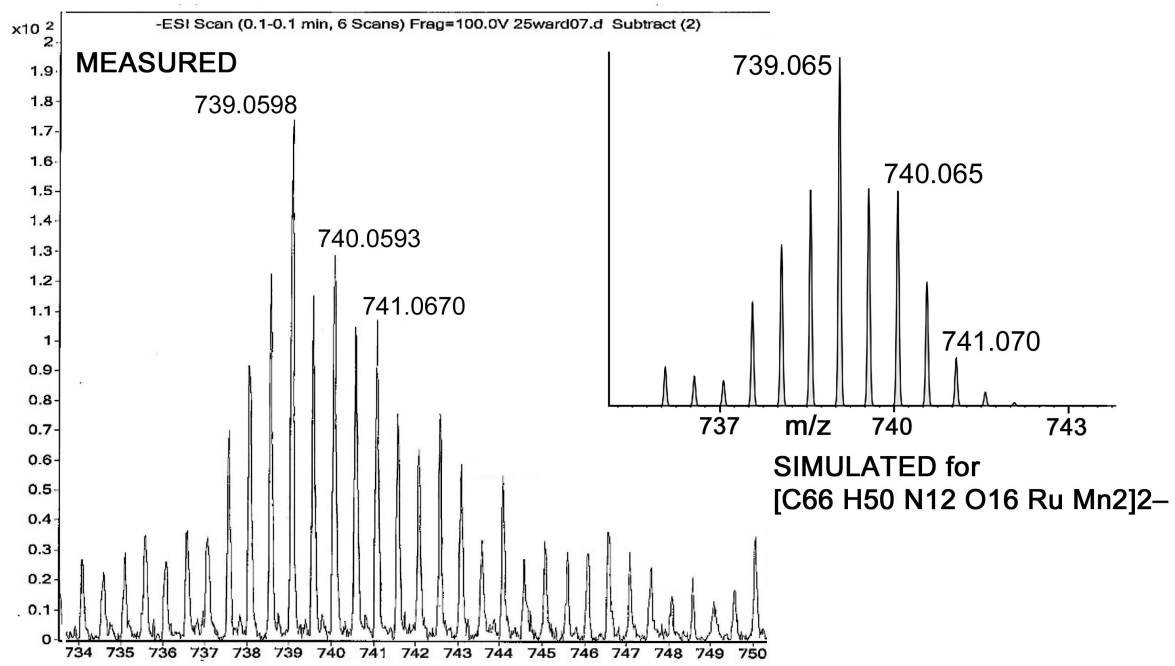

Fig. S20. Part of the high resolution ES mass spectrum of **Ru•Mn$_2$** showing the signal for $[C_{66}H_{50}N_{12}O_{16}RuMn_2]^{2-}$.

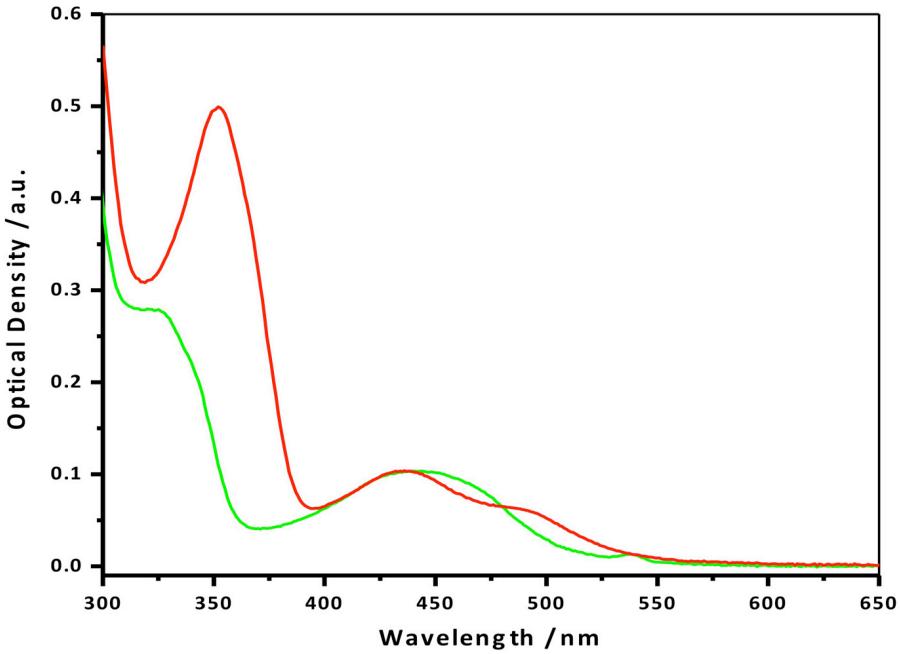

Fig. S21. UV/Vis absorption spectra in MeOH, normalised at 435 nm, of **Ru•E** (green) and **Ru•E$_2$** (red), emphasising the difference in the ^{1}MLCT absorption region (500 – 550 nm). For extinction coefficients see main text.

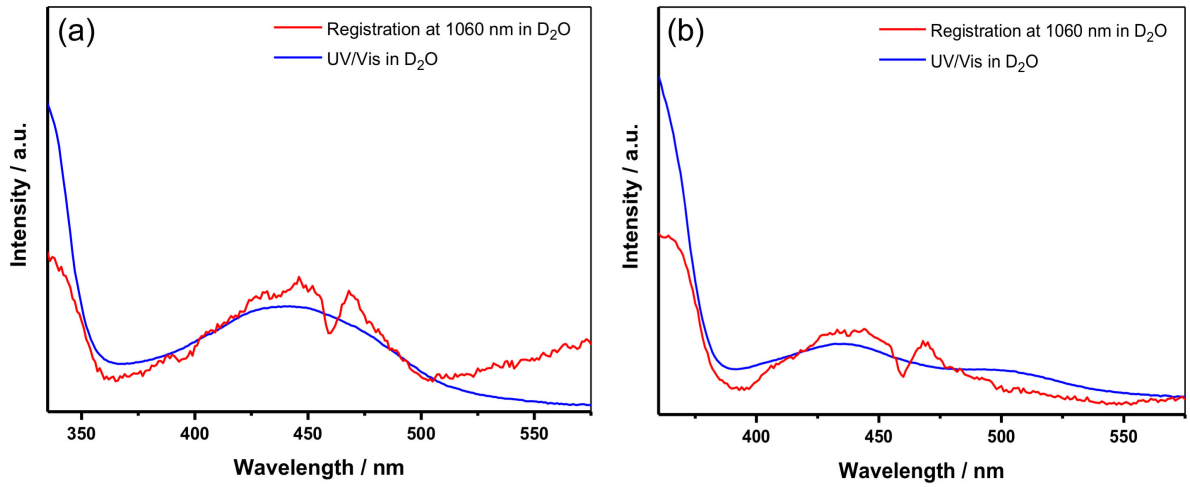

Fig. S22. Excitation spectra recorded in D_2O at 298K of (a) **Ru•Nd** and (b) **Ru•Nd$_2$**, monitoring excitation at 1060 nm in both cases, showing overlap of the main feature of the excitation spectra with the Ru-based ^{1}MLCT absorption manifold.

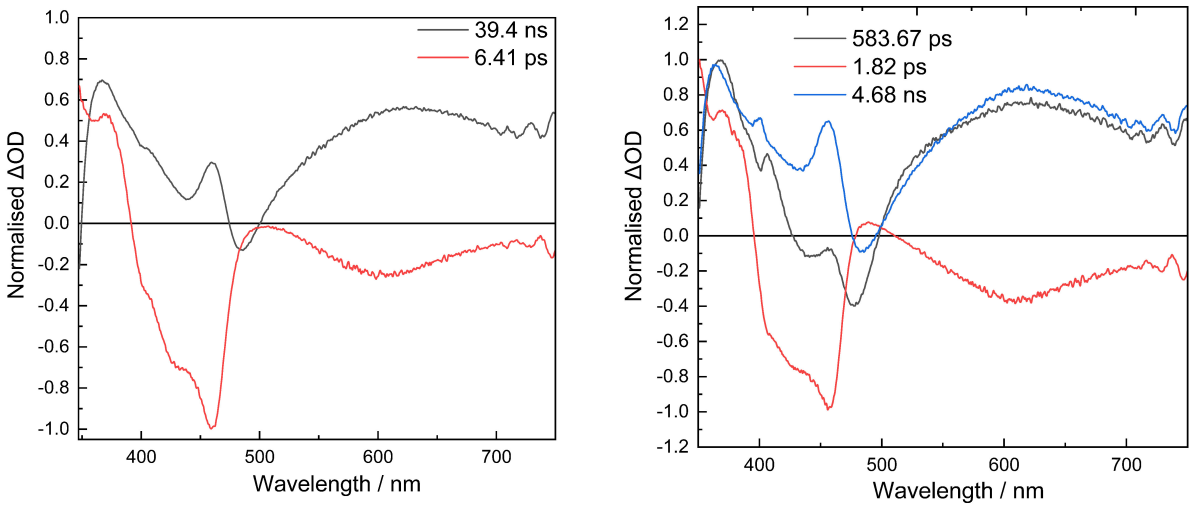

Fig. S23. Decay-associated spectra obtained by global analysis of the transient absorption spectral data of **Ru•Zn** (left) and **Ru•Mn**, in water at RT.

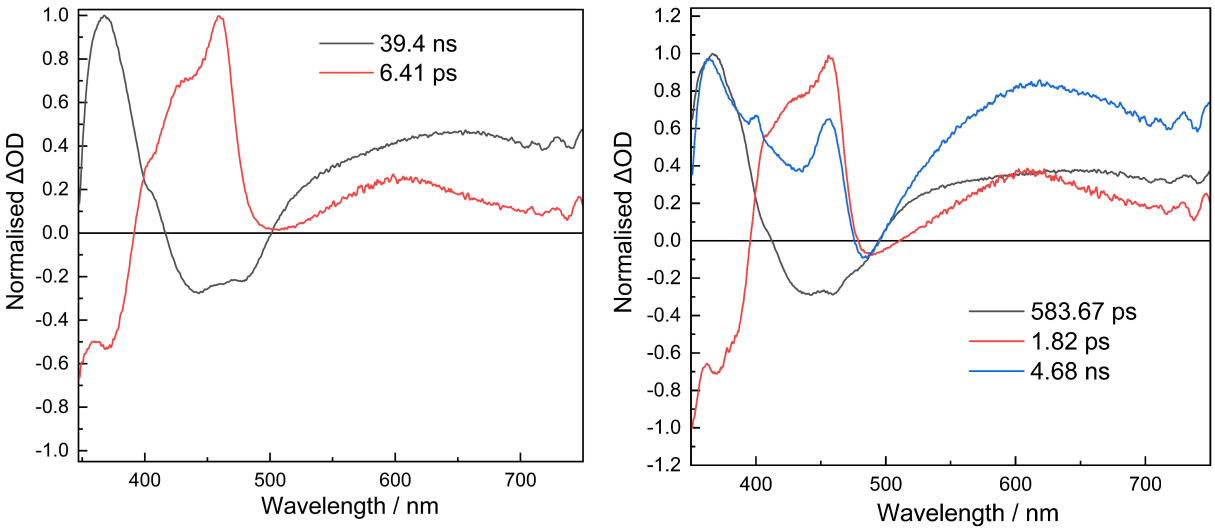

Fig. S24. Evolution-associated spectra, illustrating the appearance of the experimental TA spectra at different time delays, for **Ru•Zn** (left) and **Ru•Mn** (right), in water at RT.

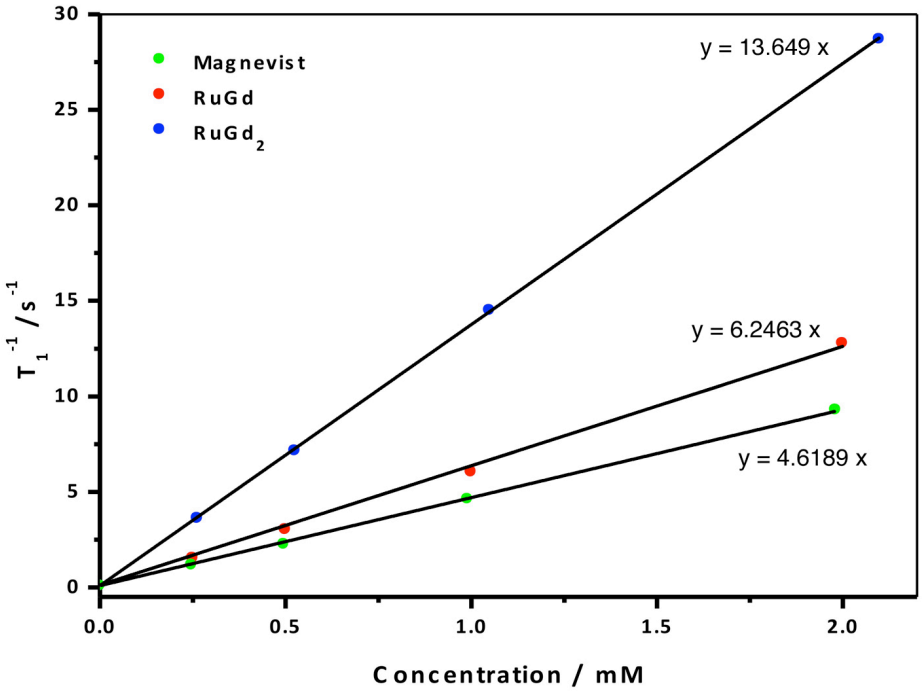

Fig. S25. Plot of relaxation rate of water protons (s^{-1}) *vs.* concentration of Gd(III)-containing complex (mM) for **Ru•Gd** (red dots), **Ru•Gd$_2$** (blue dots) and Magnevist (green dots) (400 MHz, 298 K, D_2O).

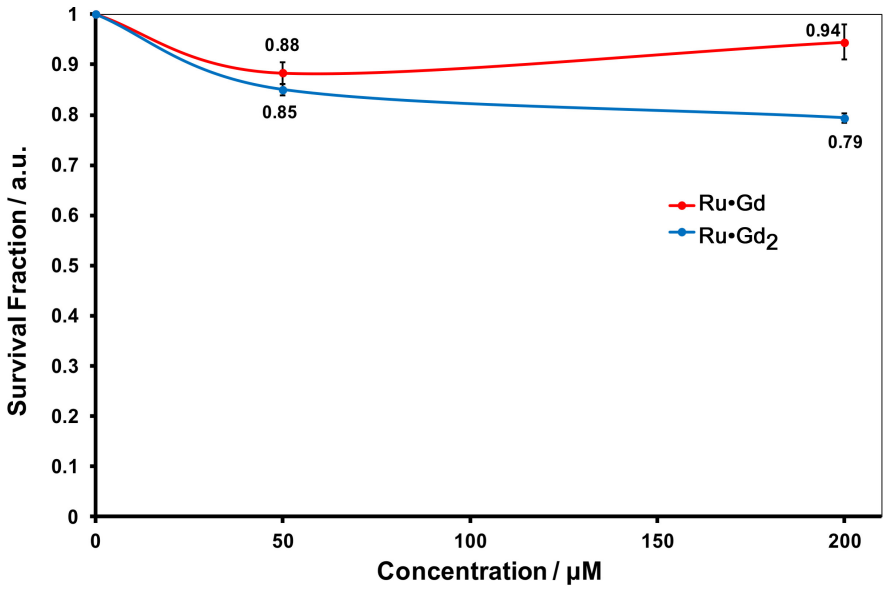

Fig. S26. Clonogenic toxicity assay of HeLa cells incubated with **Ru•Gd** (red line) or **Ru•Gd$_2$** (blue line) at concentrations of 50 μM and 200 μM for 4h. Incubations were carried out in full DMED at 37 ˚C under an atmosphere of CO_2/air (5/95, *v/v*) for 7 – 10 days until visible cell colonies had formed. Error bars represent the standard deviation of six data points (three repeats of each of duplicate datasets).

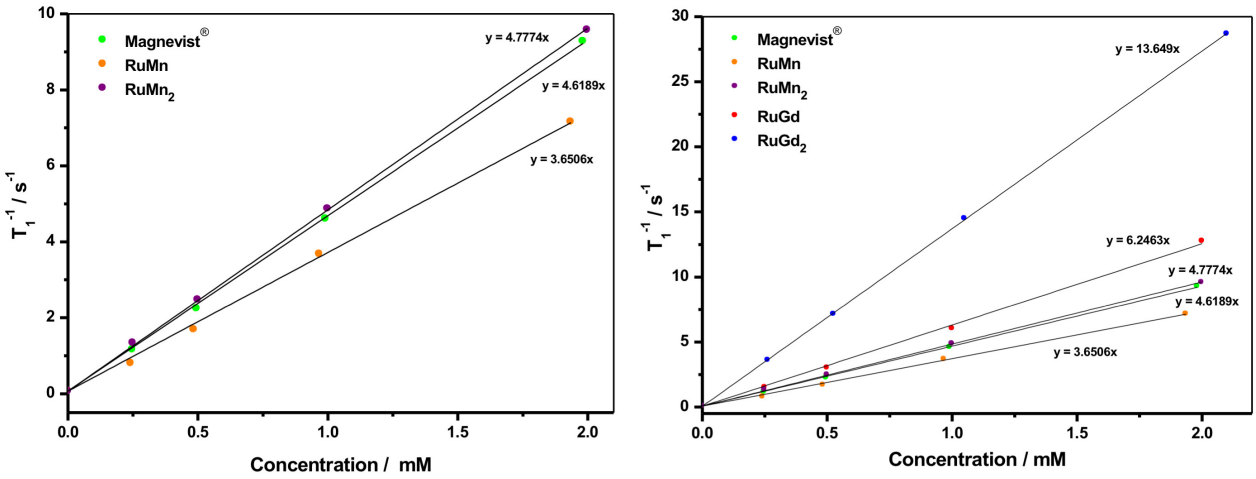

Fig. S27. Plot of concentration (mM) *vs.* relaxation rate of water protons (s^{-1}) to determine the concentration-normalised longitudinal relaxivity values for **Ru•Mn** (orange) and **Ru•Mn$_2$** (purple). The data for **Ru•Gd** (red), and **Ru•Gd$_2$** (blue) and the commercial MRI contrast agent Magnevist® (green) are also included for comparison (400 MHz, 298 K, D_2O).